

Nanoscale

Accepted Manuscript



This is an *Accepted Manuscript*, which has been through the Royal Society of Chemistry peer review process and has been accepted for publication.

Accepted Manuscripts are published online shortly after acceptance, before technical editing, formatting and proof reading. Using this free service, authors can make their results available to the community, in citable form, before we publish the edited article. We will replace this *Accepted Manuscript* with the edited and formatted *Advance Article* as soon as it is available.

You can find more information about *Accepted Manuscripts* in the [Information for Authors](#).

Please note that technical editing may introduce minor changes to the text and/or graphics, which may alter content. The journal's standard [Terms & Conditions](#) and the [Ethical guidelines](#) still apply. In no event shall the Royal Society of Chemistry be held responsible for any errors or omissions in this *Accepted Manuscript* or any consequences arising from the use of any information it contains.

ARTICLE

An ultra-sensitive impedimetric immunosensor for detection of serum oncomarker CA-125 in ovarian cancer patients

Cite this: DOI: 10.1039/x0xx00000x

M. Johari-Ahar^a, M. R. Rashidi^{a*}, J. Barar^a, M. Aghaie^a, D. Mohammadnejad^b, A. Ramazani^c, P. Karami^a, G. Coukos^{d,e} and Y. Omid^{a*}

Received 00th November 2014,
Accepted 00th XXXXX 201X

DOI: 10.1039/x0xx00000x

www.rsc.org/

Effective treatment of ovarian cancer depends upon the early detection of the malignancy. Here, we report on the development of a new nanostructured immunosensor for early detection of cancer antigen 125 (CA-125). Gold electrode was modified with mercaptopropionic acid (MPA), then consecutively conjugated with silica coated gold nanoparticles (AuNPs@SiO₂), CdSe quantum dots (QDs) and anti CA-125 monoclonal antibody (mAb). The engineered MPA|AuNPs@SiO₂|QD|mAb immunosensor was characterised using transmission electron microscopy (TEM), atomic force microscopy (AFM), cyclic voltammetry (CV) and electrochemical impedance spectroscopy (EIS). Successive conjugation of AuNPs@SiO₂, CdSe QD and anti CA-125 mAb onto the gold electrode resulted in sensitive detection of CA-125 with a limit of detection (LOD) of 0.0016 U/mL and linear detection range (LDR) of 0-0.1 U/mL. Based on the high sensitivity and specificity of the immunosensor, we propose this highly stable and reproducible biosensor for the early detection of CA-125 of the disease.

1. Introduction

Development of novel ultra-sensitive biosensor(s) provides great opportunity for quick specific sensing of cancer molecular markers (CMMs) whose early detection is of great importance for the success of cancer therapy.¹ Technically, a biosensor is an analytical device which can translate a simple biological function (e.g., interaction of two biomolecules) into a detectable electrical signal. CMMs-detecting biosensors should ideally exhibit high specificity, lower LOD and robust performance when used for determination of the desired biomarker(s) in biological fluids. Up until now, a large number of investigations have been devoted for development of highly efficient, specific and sensitive biosensors using advanced nanomaterials (NMs) and nanoparticles (NPs).²⁻⁶ Yet, biosensors remain to become substantially simplified analyzing systems for the cost-effective and robust clinical uses. One of the most important issue that needs to be taken into consideration in design and engineering of effective biosensors is the amplification of faint optical and electrochemical signals using a diverse set of advanced NMs/NPs.⁷⁻⁹

Of various NMs, AuNPs and QDs have successfully been exploited for the amplification of faint sensing signals,¹⁰⁻¹² even though little is known about their synergistic/additive benefits. Various diagnostic methods have been used for detection of CMMs involved in initiation/progression of different types of malignancies on the basis that the earlier the detection of the cancer, the higher the survival rate and the lower the morbidity rate.¹³ Despite the importance of early detection of cancer, however, the conventional analytical methods such as immunoassays used for quantitative determination of CMMs in clinic, have often failed to provide reliable outcomes. Despite providing some benefits, an immunoassay approach appears to be a time consuming process with poor precision and some difficulties towards automation. Such shortcomings may be resolved using simple and specific biosensing approaches with real time high precision capacities.¹⁴ Among several types of biosensors, electrochemical immunosensors appear to provide promising features (e.g., high specificity, simplicity and reproducibility) resulting in cost- and time-effective analysis.¹⁵ In fact, EIS is an attractive, simple and highly sensitive approach, by which the impedance is monitored as the frequency function of an applied alternative voltage showing the interfacial changes and determining the low levels of the analyte(s) bound to the surface of immunosensor.¹⁶ To improve the sensitivity of impedimetric biosensors, a vast variety of advanced NMs/NPs have been exploited.^{17, 18} Of these, immobilization of biomolecules with NPs was reported to efficiently improve the stability and to successfully preserve the activity of biomolecules.¹⁹ Of various advanced NMs, AuNPs that possess interesting physicochemical and photoacoustic properties as well as potential for surface modification (e.g., by thiol-ended entities) have been exploited for development of biosensors. While AuNPs were reported to

^a Research Centre for Pharmaceutical Nanotechnology, Faculty of Pharmacy, Tabriz University of Medical Sciences, Tabriz, Iran. Emails: rashidi@tbzmed.ac.ir ; yomidi@tbzmed.ac.ir . Fax: +98 41 33367929; Tel: +98 41 33367914

^b Drug Applied Research Centre, Tabriz University of Medical Sciences, Tabriz, Iran

^c Department of Chemical Engineering, University of Michigan, 2300 Hayward St., Ann Arbor, MI 48109, USA

^d Ovarian Cancer Research Centre, Perelman School of Medicine, University of Pennsylvania, Philadelphia, PA, USA

^e Ludwig Centre for Cancer Research, University of Lausanne, Lausanne, Switzerland

preserve the bioactivity of biological species,²⁰ they can also facilitate the direct electron transfer between redox species and bulk electrode materials and thereby enable the improved electrochemical sensing with no necessity for the electron transfer mediators. In addition to AuNPs, QDs capped with organic linkers have been reported to amplify the signals generated from the EIS analysis, upon which they offer great possibility for the covalent and efficient immobilization of biological entities with different functional groups.^{12, 21}

Although the foremost hurdle in the early detection of cancer is related to the lack of suitable CMMs, implementation of robust sensing methods with high precision and low LOD may revolutionize the treatment strategies of life-threatening malignancies such as ovarian cancer. Of various oncomarkers involved in the initiation and/or progression of ovarian cancer, mucin 16 (MUC16 or CA-125) is a blood-circulating antigen (Ag) which is a high molecular weight glycoprotein found on the surface of ovarian cancer cells.²²⁻²⁴ Given that the early sensitive detection of CA-125 is crucial for the success of ovarian cancer therapy, in the current investigation, we aimed at engineering a novel highly sensitive immunosensor specific to CA-125. To this end, we capitalised on covalent immobilization steps to construct separation free, highly stable and reproducible EIS-based immunosensor for highly sensitive detection of CA-125. Our main goal was to lower the LOD of immunosensor through simultaneous amplification of the faint signals by silica coated AuNPs and QDs.

2. Materials and Methods

2.1 Apparatus and reagents

Electrochemical measurements were performed using Potentiostat-Galvanostat Autolab station, Echo Chemie B.V., AutoLab PGSTAT302N (Metrohm Co., Schiedam, Netherlands). All experiments were carried out using a conventional three-electrode system, consisting of a gold electrode ($\varphi = 3\text{ mm}$) as the working electrode, a platinum wire as the counter electrode and Ag/AgCl (sat. KCl) as the reference electrode. All potentials were referred to the reference electrode. All experiments were performed at room temperature (20 °C). All fluorescence measurements were recorded using a RF-5301PC spectrofluorophotometer (Shimadzu Corporation, Kyoto, Japan). UV-VIS spectroscopy was fulfilled by Cecil 7500 (Cecil instruments, Cambridge, UK). The working gold electrode and pH Lab meter (827 models) were from Metrohm Co. (Schiedam, Netherlands). Hydrogen tetrachloroaurate (III) trihydrate (ACS, 99.99% metals basis, Au 49.5% min) was prepared from Alfa Aesar®. Anti-MUC16, OC125, antibody (ab693) and CA-125 oncomarker were purchased from Abcam (Cambridge, MA, USA) and Fujirebio Diagnostics, Inc. (Malvern, PA, USA), respectively. Aminopropylsilane (APS), 1-Ethyl-3-(3-dimethylaminopropyl)carbodiimide (EDC, EDAC or EDCI), N-Hydroxysuccinimide (NHS), L-cysteine (L-Cys), 3-mercaptopropionic acid (MPA) and phosphate buffer saline (PBS), sodium chloride, sulfuric acid, potassium ferrocyanide ($\text{K}_4[\text{Fe}(\text{CN})_6]$), borate buffer, potassium ferricyanide ($\text{K}_3[\text{Fe}(\text{CN})_6]$), ethanol and trisodium citrate were purchased from Merck Co., (Darmstadt, Germany). Cadmium chloride, selenium, sodium borohydride, sodium hydroxide, tris (hydroxymethyl) aminomethane, bovine serum albumin were obtained from Sigma-Aldrich Co., (Taufkirchen, Germany). The double distilled filtered (0.2 μm) water (ddH_2O) used in all the experiments in this study was prepared using Millipore

Co. (Billerica, MA, USA). Sodium silicate solution was purchased from Panreac Co. (Barcelona, Spain).

2.2 Synthesis of AuNPs

Synthesis of citrate-capped AuNPs was carried out using a previously reported method,^{25, 26} with slight modifications. Colloidal AuNPs were prepared according to the standard sodium citrate reduction method. Briefly, 18 mg of hydrogen tetrachloroauric acid (HAuCl_4) was dissolved in 100 mL of boiling deionised water and then 3 mL of sodium citrate solution (1% W/V) was rapidly added. Upon the addition of sodium citrate, the color of solution started to change from yellow to dark, which quickly subsequently turned into the bluish-gray or purple within few min. The solution was boiled for 30 min, allowing the reaction to complete and subsequently reach ambient temperature. The final color of the solution was deep wine-red. The solution contained NPs with an average size range of 15 nm in diameter characterised by TEM and UV-Vis spectrophotometry. The size and the concentration of AuNPs were also determined directly from UV-Vis absorption spectra using a method reported previously.²⁷

2.3 Preparation of AuNPs@SiO₂

For the synthesis of AuNPs@SiO₂, we used a simple method reported previously,²⁸ with some modifications. Briefly, a freshly prepared aqueous solution of APS (0.4 mL, 1.0 mM) was added to 100 mL of the AuNPs solution under vigorous magnetic stirring for the attachment of amine groups onto the surface of AuNPs. After 15 min, under vigorous magnetic stirring, 3.2 mL of sodium silicate solution (0.54% v/v, pH 10-11) was added to the colloidal mixture to coat an ultrathin layer of amorphous silica on the surface of AuNPs. The resulting dispersion (pH 8-9) was left at 80 °C for 48 h to achieve silica shell thickness of ~2-4 nm. Afterward, to remove the unreacted silicate, the colloidal mixture was centrifuged at 24000 $\times g$ for 30 min, avoiding further co-precipitation of silica nuclei. After centrifugation, AuNPs@SiO₂ were redispersed in 100 mL ddH_2O .

2.4 Synthesis of L-Cys capped CdSe QDs

For the synthesis of L-Cys capped CdSe QDs, we used a versatile method previously described with minor modification.²⁹ Briefly, 10 mL of ddH_2O was added into flask (I) and de-aerated with argon gas for 20 min under magnetic stirring. The equal molar ratio of Se and NaBH_4 was also added into a 100 mL round-bottom flask II, and then the oxygen free ddH_2O of flask (I) was added to the flask (II) to complete the reaction at 40 °C for 30 min (reaction [1]). Also, a designated amount of 0.02 M CdCl_2 and 0.0012 M L-Cys (20 mL each) were added into another 100 mL round-bottom flask (III) and pH of solution was adjusted at 11. This solution was also de-aerated with argon gas for 30 min by stirring (reaction [2]). Finally, an adequate amount of reaction [1] was added into flask (III) to make the Se/Cd molar ratio of 0.75, and then the flask (III) was sealed and refluxed for 60 min. The L-Cys capped CdSe QDs were obtained through ethanol precipitation (1:1 v/v) by centrifugation at 4000 $\times g$ for 5 min. The QDs were then washed (3 \times) with absolute ethanol. The size and concentration of CdSe nanocrystals were determined using a method published previously.³⁰

2.5 Gold electrode cleaning

The working electrodes were orderly polished by slurry alumina (0.05, 0.3 and 1.0 μm) and polishing cloth for 2 min.

Then, the electrodes were rinsed with ddH₂O, and cleaned ultrasonically in a 1:1 mixture of ethanol:water for 5 min to remove the residual of alumina particles that might be adsorbed on the surface of electrodes. To remove any possible impurities, the electrodes were further immersed in a piranha solution (3:1, sulfuric acid:hydrogen peroxide) for 10 min, and subsequently rinsed with a mixture of ethanol and ddH₂O (1:1 v/v). The electrodes were then subjected to potential cycling (0.0–1.5 V, 100 mV s⁻¹) in a 1.0 M aqueous HClO₄ for 20 cycles.

2.6 Self-assembled monolayer of MPA on the gold electrode surface

All the fabrication steps of CA-125 specific immunosensor are schematically illustrated in Fig. 1. The cleaned bare gold electrode was immersed in 20 mM aqueous solution of MPA (pH 7.4; adjusted by 1.0 M sodium hydroxide solution) under shaking (60 rpm) at room temperature and dark for 18 h. During this period, self-assembly of MPA monolayer on the gold electrode surface was formed through thiolation reaction (Fig. 1, step 1).

2.7 Covalent conjugation of amine-functionalized AuNPs@SiO₂

AuNPs@SiO₂ (4.0 mL) was first functionalised with amine groups (Fig. 1, step 2) by treating with 100 μL of 1.0 mM APS for 15 min, as reported previously.³¹ Then, the carboxylic groups of MPA on the surface of gold electrode were activated using EDC and NHS chemistry. Briefly, the MPA-modified electrode was washed with ddH₂O, and then activated using EDC (20 mg/mL) and NHS (10 mg/mL) and kept under shaking (60 rpm) at room temperature and dark for 1 h. The activated surface was conjugated with amine-functionalised AuNPs@SiO₂ at room temperature and dark overnight, forming the MPA|AuNPs@SiO₂ modified gold electrode (Fig. 1, step 3).

2.8 Covalent attachment of L-Cys capped CdSe QDs to the AuNPs@SiO₂ modified electrode

For the covalent binding of the acid-terminated L-Cys capped CdSe QDs, the carboxylic groups of QDs (4 mL) were activated using 50 μL EDC (20 mg/mL) and NHS (10 mg/mL) in borate buffer solution (pH 9) under shaking (60 rpm) at room

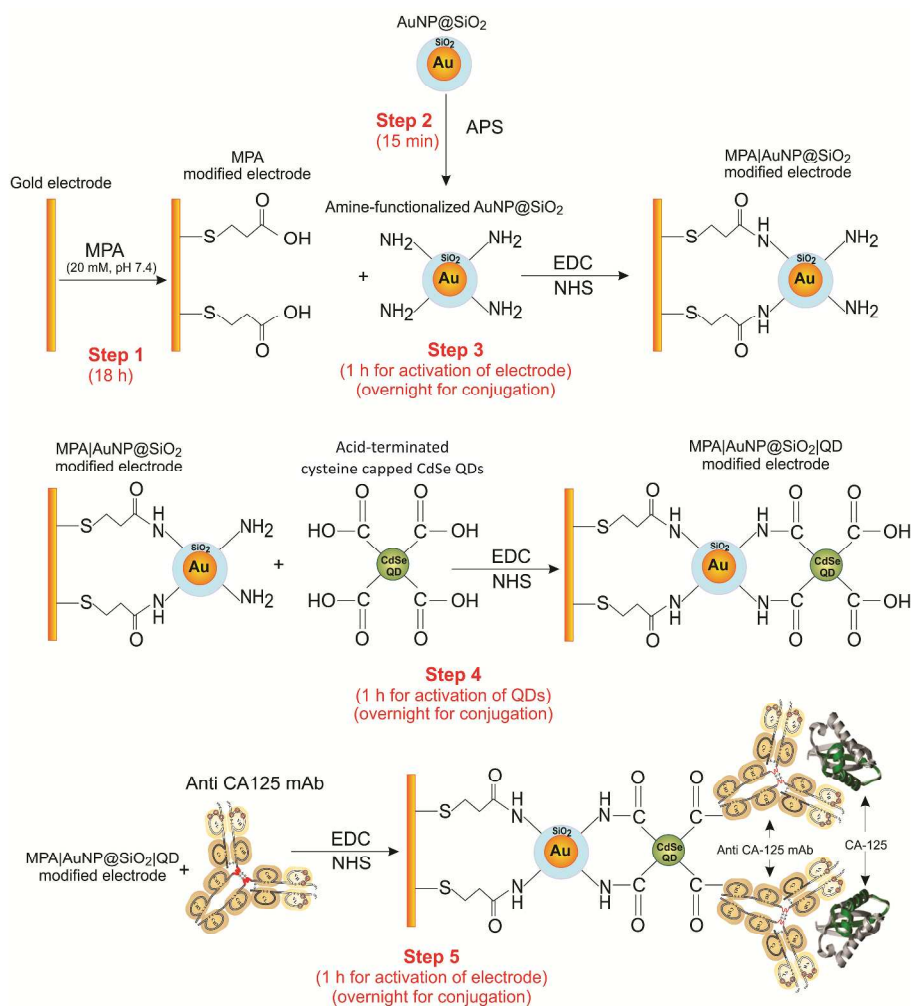


Fig. 1 Schematic representation for the engineering processes of CA-125 immunosensor. Step 1, the surface of gold electrode was functionalized with mercaptopropionic acid (MPA) to present carboxylic groups. Steps 2, AuNPs@SiO₂ were functionalized to present amine groups. Steps 3, amine-functionalized AuNPs@SiO₂ were covalently conjugated onto the MPA modified gold electrode. Step 4, acid-terminated QDs were covalently conjugated onto the MPA|AuNPs@SiO₂ modified gold electrode. Step 5, CA-125 mAbs were covalently conjugated onto the MPA|AuNPs@SiO₂|QD modified gold electrode to engineer the MPA|AuNPs@SiO₂|QD|mAb modified gold electrode.

temperature and dark for 1 h. For the covalent conjugation of the activated QDs, the MPA|AuNPs@SiO₂ modified gold electrode was incubated with the activated QDs at room temperature and dark overnight, forming the MPA|AuNPs@SiO₂|QD modified gold electrode (Fig. 1, step 4).

2.9 Antibody conjugation

Carboxylic functional groups of L-Cys on the surface of MPA|AuNPs@SiO₂|QD modified gold electrode was activated using 50 μ L EDC (20 mg/mL) and NHS (10 mg/mL) in borate buffer solution (pH 9) under shaking (60 rpm) at room temperature and dark for 1 h. For the covalent conjugation of anti-CA-125 mAb, the activated electrode was incubated with the mAb at room temperature and dark overnight, forming the MPA|AuNPs@SiO₂|QD|mAb modified gold electrode (Fig. 1, step 4). Furthermore, the non-specific bonding sites at the surface of MPA|AuNPs@SiO₂|QD|mAb modified gold electrode were blocked by incubation of the electrode in 2% BSA solution at 4 °C for 60 min.

2.10 AFM analysis

To perform AFM analysis, all the fabrication steps of biosensor were simulated on the glass slide. First, the glass slide was cleaned with acetone and rinsed with Milli-Q water (18.2 Mega Ω -cm at 25 °C). Then, the glass slide was dried under nitrogen flow and further necessary modifications were applied. Firstly, the glass slide was immersed in the solution of carboxymethyl triethoxysilane (20 mM) at room temperature for 48 h in order to react the silane with hydroxyl groups on the surface of glass slide. Carboxyl groups of silanizing agent at the surface of glass were activated by EDC/NHS (1:1, 20 mM) for 1 h and reacted with amino functionalised silica coated AuNPs at room temperature for 24 h. Secondly, using EDC/NHS (1:1, 50 μ M) activation process, L-Cys capped QDs were attached to the AuNPs@SiO₂ modified glass slide to form AuNPs@SiO₂|QD modified glass slide. For the conjugation of anti-CA-125 mAb (to form the AuNPs@SiO₂|QD|mAb modified glass slide), 500 μ L of mAb (0.2 μ g/ μ L) were conjugated onto the modified glass slide using EDC/NHS activation process through incubation at 8 °C overnight. All AFM experiments were performed at contact mode by Nanowizard AFM (JPK Instruments AG, Berlin, Germany) mounted on Olympus Invert Microscope IX81 (Olympus Co., Tokyo, Japan). We used silicon nitride cantilever (length of 200 μ m, width of 22 μ m and thickness of 0.6 μ m, Applied Nano Structures, Inc., Mountain View, CA, USA) and silicon tip (HYDRA6V-200N, Applied Nano Structures, Inc., Mountain View, CA, USA) with spring constant of 0.045 N/m and 17–21 kHz resonant frequencies. All images were acquired in air at ambient condition with the scan rate of 1–2 Hz, and processed by image leveling to eliminate the background slope and adjust the contrast and brightness using Nanowizard software (JPK Instruments AG, Berlin, Germany).

2.11 Electrochemical measurements

All electrochemical measurements were performed using a PC controlled PGSTAT302N Autolab equipped with frequency response analyzer (FRA) module. CV and EIS experiments were performed in the solution containing 5 mM K₃[Fe(CN)₆]/K₄[Fe(CN)₆] (1:1) and PB (0.1 M, pH 7) using a conventional three-electrode configuration system. For the CV analysis, the potential was cycled from –0.1 to 0.6 V with the scan rate of 100 mVs⁻¹. The EIS measurements were performed

within a frequency range of 0.1 Hz to 100 kHz at the formal potential of redox couple Fe(CN)₆^{4-/3-} (0.17 V). The impedance data were represented in the form of complex plot (Nyquist plot), and the fitting program of AUTO-LAB (Nova 1.8) was used to analyse the impedance spectra through an appropriate equivalent electrical circuit.

2.12 Characterization of immunosensor by CV and EIS analyses

The fabrication process of CA-125 specific immunosensor in each step was evaluated by CV and EIS analyses. The surface of working electrode monitored by CV and EIS analyses in each step of modification included bare gold electrode, MPA modified gold electrode, MPA|AuNPs@SiO₂ modified gold electrode, MPA|AuNPs@SiO₂|QD modified gold electrode, MPA|AuNPs@SiO₂|QD|mAb modified gold electrode and Ag incubated electrode (MPA|AuNPs@SiO₂|QD|mAb modified gold electrode interacted with CA-125 molecules.

2.13 Specificity of the biosensor

In order to investigate the specificity of the prepared CA-125 specific immunosensor, EIS analysis was conducted to measure the response of immunosensor towards its cross reactivity with other ovarian cancer markers including carcinoembryonic Ag (CEA, 50 ng/mL) and α -1-fetoprotein (AFP, 50 ng/mL) in the presence/absence of human albumin serum (HSA, 10 mg/mL) in comparison with CA-125.³²

2.14 Stability and reproducibility of the biosensor

The stability assessment of the immunosensor was carried out by recording the R_{et} values at a fixed concentration of CA-125 (50 mU/mL) for a designated period of 1-3 weeks. For the physicochemical stability assessment, the immunosensor was stored in 10 mM PBS buffer solution and 0.1% sodium azide at 4 °C. The reproducibility of CA-125 immunosensor was evaluated with intra- and inter-assay precision. The intra-assay precision was assessed by measuring a fixed concentration of CA-125 for six times by a single immunosensor after regenerating. The inter-assay precision was determined by measuring the same sample of CA-125 with six different CA-125 specific immunosensors fabricated at one batch, as reported previously.³³

2.15 Precision of the CA-125 immunosensor

For the precision assessment, we capitalised on the variation coefficient (CV) of the intra-assay and inter-assay. For the intra-assay CV, the engineered CA-125 immunosensor was assessed via determining the CA-125 content of five different samples with CA-125 concentrations at 10, 30, 50, 70 and 90 (mU/mL) for three replicates after regenerating the immunosensors each time. For the inter-assay CV analysis, six CA-125 immunosensors were selected from different batches and evaluated with one fixed concentration of CA-125 (60 mU/mL), as reported previously.³⁴

2.16 Regeneration of immunosensor

The regeneration assessment of any immunosensor using rapid and easy method(s) is a critical step. Because of the non-covalent nature of Ab and Ag interaction, it should be pointed out that such immunoreaction is the basis of the regeneration process. Further, the regenerating reagents and solutions must preserve the bio-function of immobilised Ab and/or Ag without any destructive impact(s) on the structure and function of immunosensor. Among different regenerating reagents, the

regeneration efficiency of H_3PO_4 , Gly-HCl, acetonitrile (30%), DMSO (50%) and NaCl (0.5 M) have been examined in some studies previously,^{33, 35} which were the basis of the regeneration assessment in this study.

2.17 Calibration and LOD of the immunosensor

Under an optimised experimental condition, calibration graphs were plotted for the CA-125 specific immunosensor in the buffer solution (5 mM $\text{K}_3[\text{Fe}(\text{CN})_6]/\text{K}_4[\text{Fe}(\text{CN})_6]$ in PB, pH 7). A standard addition method was recruited for determination diluted or undiluted real samples by addition of designated amount of CA-125. The slope of calibration graphs in the buffer solution, diluted or undiluted real samples were compared through t-test assay or one-way ANOVA followed by a post-hoc multiple comparison analysis. Based on the CA-125 detection range of the immunosensor (0.001-10 U/mL) and the concentration range of CA-125 in clinical samples (0-400 U/mL), it is necessary to compare the diluted and undiluted real samples calibration curves to obtain a validated calibration graph for real laboratory analysis. Three times standard deviation of the blank divided to the slope of calibration plot was calculated as a LOD in two different kinds of sample analyses.³⁶ A LOD with 10-fold difference was considered as the limit of quantification.

2.18 Determination of CA-125 in human serum samples

Two assays were exploited to evaluate the diagnostic applicability and precision of the CA-125 specific immunosensor towards detection of CA-125 in human serum samples obtained from Nomooneh Laboratories (Tabriz, Iran). In the first assay, the determination of CA-125 was performed in spiked human serum species and the concentration of CA-125 was calculated from the related calibration graph. In the second experiment, the patient's samples diluted with buffer (5 mM; $\text{K}_3[\text{Fe}(\text{CN})_6]/\text{K}_4[\text{Fe}(\text{CN})_6]$ in PB, pH 7.0) was used to attain the content of CA-125. The CA-125 quantification results obtained by the immunosensor (with consideration of the dilution factors) were compared with that of the analogous samples measured by the enzyme-linked immunosorbent assay (ELISA) kit, CanAg (Fujirebio Diagnostics, Inc., Malvern, PA, USA) as a conventional clinical method for the analysis of CA-125.

2.19 Statistical analysis

For the statistical analysis, we capitalised on either t-test or one-way ANOVA followed by a multiple comparison analysis (using SPSS ver. 19.0) with a p value less than 0.05.

3. Results

3.1 Characterization of engineered NPs

Fig. 2 shows the UV-Vis absorption spectra of AuNPs before and after coating with silica shell. TEM micrograph confirmed a size range of ~20 nm for the engineered AuNPs with fine silica shell (Fig. 2, inset). Once coated with SiO_2 , AuNPs showed a red shift to 550 nm (from 530 nm) in the UV-Vis absorption spectra. Fig. 3 represents the UV-Vis absorption spectra of CdSe QDs indicating a distinguished excitonic absorption peak at 460 nm, which were further analysed using TEM (Fig. 3, inset a) and fluorescence spectroscopy captured after 2 h reflux time indicating emission peak at 560 nm (Fig. 3, inset b). It should be pointed out that the size of engineered QDs is tunable with the reflux time (see Fig. S1, Electronic Supplementary Information).

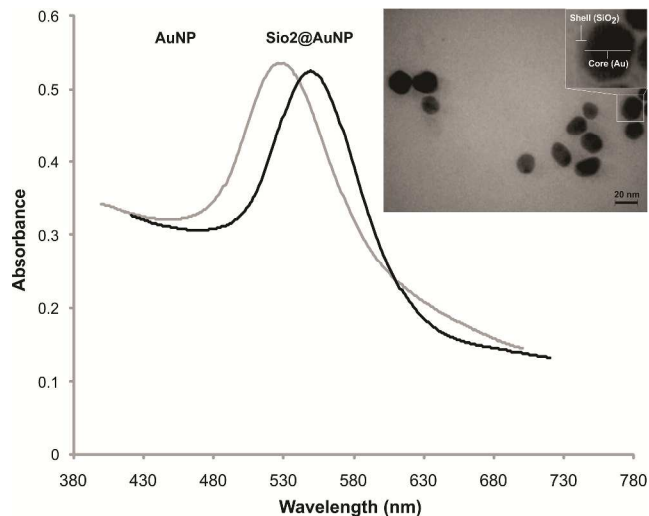


Fig. 2 UV-Vis absorption spectra of AuNPs and AuNPs@ SiO_2 . Inset: TEM micrograph of AuNPs@ SiO_2 and the magnification of single AuNPs@ SiO_2 .

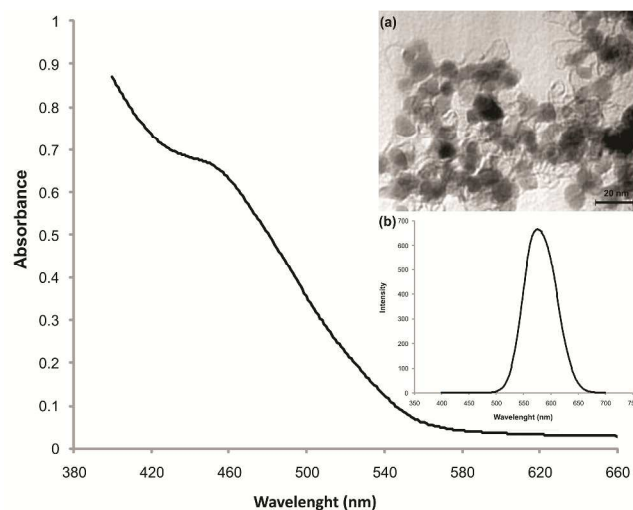


Fig. 3 UV-Vis absorption spectra of CdSe QDs. Inset: TEM micrograph (a) and fluorescence spectrum of CdSe QDs (b).

3.2 AFM analyses

Figs. 4, 5 and 6 respectively represent the surface architecture of AuNPs@ SiO_2 , AuNPs@ SiO_2/QD , and AuNPs@ $\text{SiO}_2/\text{QD}/\text{mAb}$ modified glass slides. The AFM micrographs substantiated the morphological arrangement of AuNPs, QDs and mAbs on the surface of glass slides. To fully characterise the surface modification of the immunosensor, we capitalised on the contact mode AFM analysis to acquire high-resolution images, including: (a) height, (b) deflection (error signal), (c) line profile, and (d) three dimensional (3D) images. AuNPs were found to be successfully conjugated on the surface of the glass slide through an amide bound (Fig. 4). We performed AFM using the contact mode to ensure upon the architecture and dimension of the modification though mode may somewhat distort the samples. The height of AFM images (Figs 4A, 5A and 6A), the deflection images (Figs 4B, 5B and 6B) together with 3D images (Figs. 4C, 5C and 6C) all confirmed the well-oriented modifications of the surface by AuNPs, QDs and mAbs, respectively. These results were revalidated using non-contact mode imaging (data not shown).

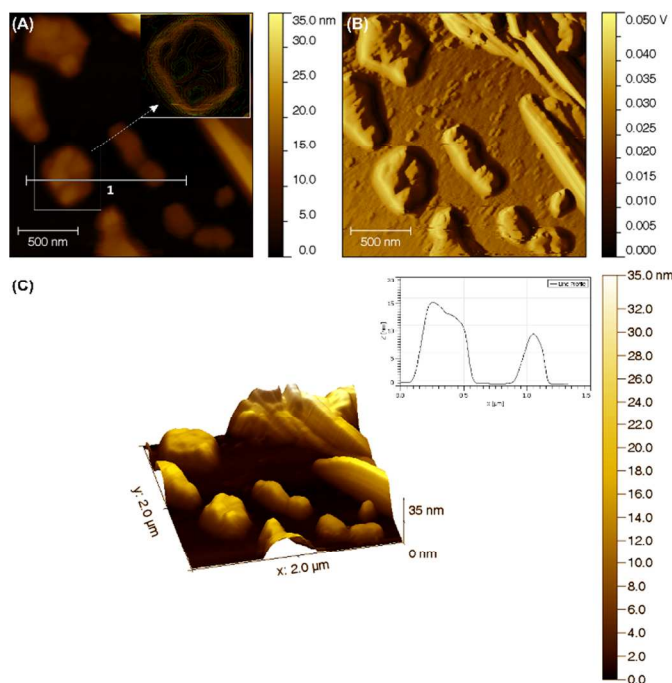


Fig. 4 Contact mode AFM topography of MPA|AuNPs@SiO₂ modified gold electrode. A) The height measured image. B) The error signal image. C) The 3D image with line profile format (inset). White arrow (panel A) indicates the edge detection pattern and horizontal numbered line 1 (panel A) refers to the path of line profile image whose histogram is shown in panel C (inset). Images were acquired using JPK AFM instrument equipped with silicon tip (HYDRA 6V-200N) at a scan rate of 1-2 Hz.

3.3 CV analyses

The surface properties of the gold electrode at each modification step were characterised by means of electrochemical analyses. The cyclic voltammogram of a fairly reversible redox couple (i.e., Fe(CN)₆^{4-/3-}) was selected as a probe to investigate the characteristics of gold electrode in each assembly step.

As presented in Fig. 7, Fe(CN)₆^{4-/3-} showed the reversible behavior on the bare gold electrode (Fig. 7, curve a). Moreover, MPA effectively blocks the interfacial electron transfer between the redox couples in the solution and the gold electrode surface (Fig. 7, curve b).

Once the MPA modified gold electrode was functionalised with AuNPs@SiO₂, the electron transfer rate was improved efficiently (Fig. 7, curve c). Additional increase in current was observed upon the conjugation of MPA|AuNPs@SiO₂ modified gold electrode with CdSe QDs (Fig. 7, curve d). However, the current of redox couple was decreased by the immobilization of anti CA-125 mAb onto the MPA|AuNPs@SiO₂|QD modified gold electrode (Fig. 7, curve e).

3.4 EIS analyses

The EIS data can be interpreted by fitting with Randles equivalent circuit (see Table S1, Electronic Supplementary Information). As shown in Fig. 8 (inset), this circuit consists of (a) ohmic resistance of the electrolyte solution (R_s) in series with the parallel combination of the double-layer capacitance (C_{dl}) and (b) an impedance of a faradaic reaction (R_{et}) which is in series with Warburg impedance (Z_W).

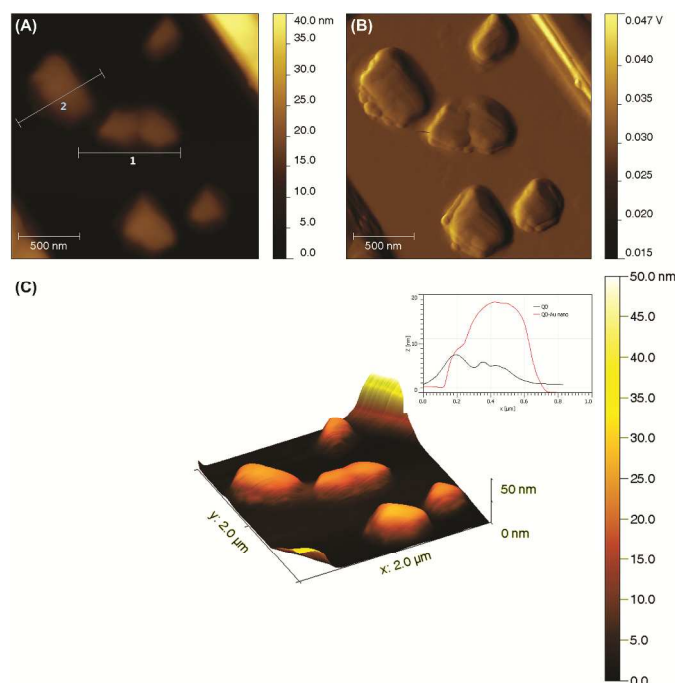


Fig. 5 Contact mode AFM topography of MPA|AuNPs@SiO₂|QD modified gold electrode. A) The height measured image. B) The error signal image. C) The 3D image with line profile format (inset). Numbers (1 and 2 in panel A) refers to the path of line profile image whose histograms are shown in panel C (inset). Images were acquired using JPK AFM instrument equipped with silicon tip (HYDRA 6V-200N) at a scan rate of 1-2 Hz.

The bare gold electrode exhibited a small semicircle in the Nyquist plot (Fig. 8, curve a). Once MPA assembled on the bare gold electrode, a higher interfacial R_{et} was observed in the impedance spectrum (Fig. 8, curve b). Next, the covalently attached amine-functionalised AuNPs@SiO₂ with carboxyl group of MPA was found to promote the electron transfer process (Fig. 8, curve c). Further, the R_{et} value was decreased by the conjugation of carboxylic acid functionalised CdSe QDs (Fig. 8, curve d). Once the CA-125 mAb conjugated onto the electrode surface (Fig. 1), the R_{et} value was significantly increased (Fig. 8, curve e).

3.5 The effect of the incubation temperature and time

The effect of incubation temperature on optimum Ag-Ab immunoreaction was explored by the immersing of immunosensor in 50 μU/mL of CA-125 oncomarker for 60 min at different incubation temperatures (i.e., 8, 20, 30, 37, 40 and 50 °C). Based upon impedimetric electrochemical responses, the best temperature was found to be 37 °C (see Fig. S2, Electronic Supplementary Information). To investigate the influence of the incubation time on the performance of the immunosensor, the finally modified electrode was immersed in 50 μU/mL of CA-125 at 37 °C for different time points (20, 40, 60, 90, 120 and 150 min) under shaking at 60 rpm. An increase in the incubation period was found to enhance the electrochemical response. The plot reached a plateau when the immunological reaction time was longer than 60 min, hence this time period (60 min) was determined as an optimum time (see Fig. S3, Electronic Supplementary Information).

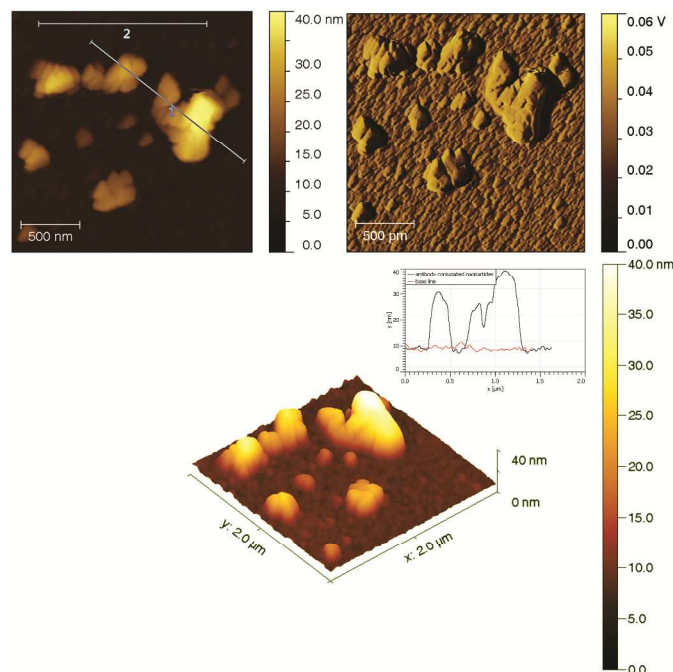


Fig. 6 Contact mode AFM topography of MPA|AuNPs@SiO₂|QD|mAb modified gold electrode. A) The height measured image. B) The error signal image. C) The 3D image with line profile format (inset). Numbers (1 and 2 in panel A) refers to the path of line profile image whose histograms are shown in panel C (inset). Images were acquired using JPK AFM instrument equipped with silicon tip (HYDRA 6V-200N) at a scan rate of 1-2 Hz.

3.6 Specificity of the biosensor

For further evaluation of immunosensor, the specificity of the immunosensor was evaluated in the presence of HSA, CEA and AFP. Fig. 9 shows the EIS analysis of the immunosensor in the presence of these counterparts. The R_{et} values for HSA, CEA and AFP were significantly ($p < 0.05$) lower than that of the CA-125, similar to that of the blank samples ($R_{et} = 992.97 \pm 2.59$). The impedimetric response of the immunosensor to CA-125 was also found to correlate with an increase in the concentration of CA-125. These data clearly imply that the immunosensor can specifically sense the target oncomarker, CA-125.

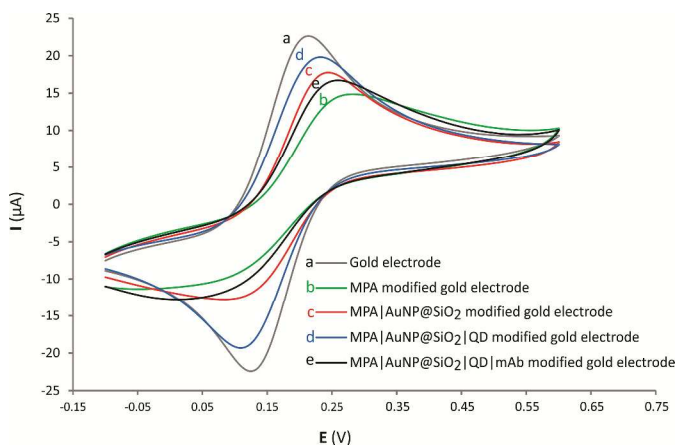


Fig. 7 CV spectra of different modification steps. CV analyses were performed at -0.1 to 0.6 V in 5 mM $K_3[Fe(CN)_6]/K_4[Fe(CN)_6]$ in phosphate buffer, pH 7.

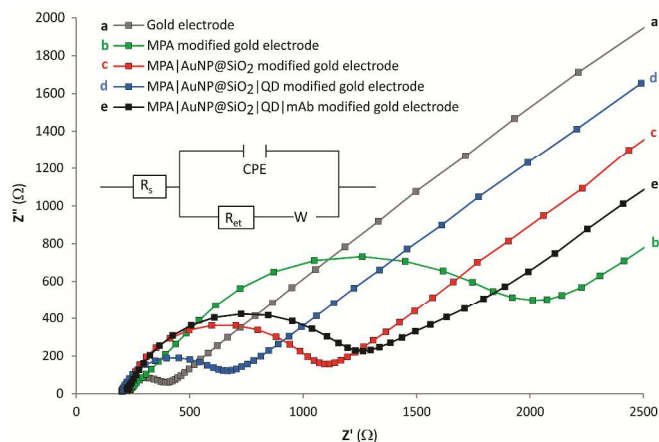


Fig. 8 Electrochemical impedance spectroscopy of different modification steps. EIS measurements were performed in 5 mM $K_3[Fe(CN)_6]/K_4[Fe(CN)_6]$ in phosphate buffer, pH 7, using a bios voltage of 0.17 V and the frequency range of 0.1 Hz to 100 kHz. The inset is the equivalent circuit used to model impedance data in the form of R_s , Z'' , R_{et} and CPE, respectively.

3.7 Stability and reproducibility of the immunosensor

The stability and reproducibility of the immunosensor were tested during a period of 3-week. The reactivity of the immunosensor with the target oncomarker CA-125 was found to show exactly similar profile during this period of storage. The R_{et} values showed less than 10% ($n=5$) deviation, revealing that the engineered immunosensor possesses long-term and acceptable stability (see Fig. S4, Electronic Supplementary Information).

3.8 Precision of the CA-125 immunosensor

To analyse the detection accuracy of immunosensor, we performed both intra-assay and inter-assay. Fig. 10 represents the immunosensor responses (based on EIS data) to various concentrations of CA-125. The intra-assay CV% for the immunosensor at CA-125 concentrations of 10, 30, 50, 70 and 90 (mU/mL, $n=3$) were respectively 3.3, 4.9, 4.3, 5.2 and 4.6%. The inter-assay CV% of six different CA-125 specific immunosensors used independently was 6.2% at 60 mU/mL ($n=5$). Taken all, it is clear that the precision and the reproducibility of the engineered immunosensor were satisfactorily adequate.

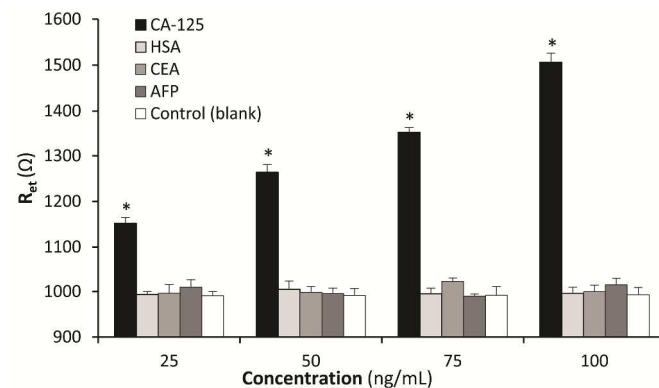


Fig. 9 Specificity assessment of MPA|AuNPs@SiO₂|QD|mAb modified gold electrode immunosensor. R_{et} of CA-125 specific immunosensor for CA-125, CEA, HSA, AFP and blank samples was measured to show the specificity of the immunosensor. Asterisk represents significant difference ($p < 0.05$) of the R_{et} of CA-125 analysed by the engineered immunosensor.

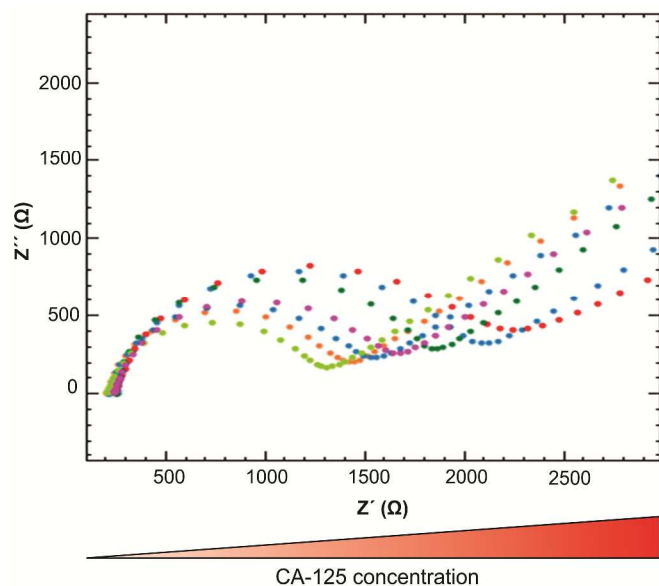


Fig. 10 The response of EIS-based immunosensor to various concentrations of CA-125. The diameter of the semicircle of Nyquist plot represents a direct correlation with the concentration of CA-125.

3.9 Regeneration of immunosensor

For the regeneration of engineered immunosensors, we utilised glycine-HCl (0.15 M, pH 2.0) in two regeneration cycles for 3 min. The immunosensor displayed regeneration efficiency of $98\% \pm 1.2$ ($n=5$) up to 22 cycles with an acceptable reproducibility and precision. In our study, the engineered immunosensors were regenerated in the fixed concentration of CA-125 (i.e., 40 mU/mL).

3.10 Calibration and recovery of immunosensor

To calibrate the immunosensor, impedimetric responses were measured in various concentrations of CA-125 from 1.0 to 10.0 U/mL (see Fig. S5 and Table S2, Electronic Supplementary Information). The EIS analysis was performed using $\text{Fe}(\text{CN})_6^{3-}$ in PB solution and the results revealed that the response of immunosensor was proportional to the concentration of CA-125. Hence, it can be inferred that the higher the concentration of CA-125, the greater the diameter of the semicircle part in the Nyquist plot.

Further, recovery ranges of the immunosensors were between 91.2 and 100.5% with RSD 0.94-1.68%, which are within acceptable range. It should be pointed out that the acceptable recovery of 10 ppm level is around 80–110% with RSD of 7.3–11.3%.³⁷

3.11 Real sample analysis

The potential application of developed immunosensor was investigated by measuring the CA-125 concentration in the serum of ovarian cancer patients. The engineered immunosensor showed great detection potential in comparison with ELISA (Table 1). We found that there is no significant difference between the results obtained from the engineered EIS-based immunosensor and ELISA method ($p < 0.05$).

Further, it should be highlighted that the presence of proteins other than CA-125 in the serum showed no remarkable effect(s) on the sensitivity and specificity of the EIS-based biosensing of CA-125.

Table 1 Quantification of CA-125 in human serum samples by the EIS-based immunosensor (considering dilution factor, DF) in comparison with ELISA method ($n=3$)

| Patients samples | ELISA (U/mL) | RSD (%) | EIS (U/mL) | DF | RSD (%) |
|------------------|--------------|---------|------------|-------|---------|
| 1 | 83 | 2 | 81 | 1000 | 2 |
| 2 | 168 | 3 | 164 | 10000 | 2.5 |
| 3 | 240 | 1 | 243 | 10000 | 3.2 |
| 4 | 105 | 4 | 103 | 10000 | 2 |
| 5 | 155 | 2 | 154 | 10000 | 1.2 |
| 6 | 452 | 1 | 451 | 10000 | 3.3 |
| 7 | 95 | 1 | 92 | 1000 | 2.1 |
| 8 | 133 | 3 | 133 | 10000 | 1 |
| 9 | 344 | 2 | 348 | 10000 | 4.1 |
| 10 | 198 | 1 | 197 | 10000 | 3 |

4. Discussion

Cancer is a multifaceted-disease with unique molecular biosignature,³⁸⁻⁴⁰ whose clear-cut detection at the early stage of disease using a simple and effective diagnosis method may significantly enhance the survival of cancer patients. Ovarian cancer, as one of the most life-threatening malignancies among women worldwide, is usually diagnosed at the late stage despite upregulation of molecular markers such as CA-125 at the early stages of the malignancy.

Up until now, several quantitative methods have been developed for the determination of CA-125 within serum samples of ovarian patients. Currently, ELISA and chemiluminescence are common methods for the quantification of CA-125 in clinic.^{41, 42} Although these methods are reliable and reproducible diagnostic approaches, they demand tedious laborious works and may also associate with nonspecific binding as well as inappropriate LODs. Further, the routine techniques used in clinic for the quantification of CA-125 provide LODs at a range of 1.0 U/mL, therefore they are hardly able to detect low concentration of CA-125 important for the early diagnosis of malignancy. To improve the CA-125 LOD value, in the current study, we designed and developed a sensing platform by capitalizing on a gold electrode decorated with AuNPs, CdSe QDs and anti CA-125 mAb (Fig. 1). We assumed that such immunosensor can amplify the faint signals, which is a critical step for the detection of trace amount of CA-125.

The synthesised NPs were characterised using UV-Vis absorption spectroscopy and TEM analyses. Upon coating AuNPs with SiO_2 , their UV-Vis absorption peak was shifted to 550 nm from 530 nm (Fig. 2), indicating an increase in the intensity of plasmon absorption by AuNPs@ SiO_2 . This observation is in accord with the previous reports, highlighting the impact of silica shells on the enhancement of the local refractive index around AuNPs.⁴³ The UV-Vis absorption analysis showed a distinguished excitonic absorption peak at 460 nm for CdSe QDs (Fig. 3), whose epitomic nanostructured morphology was confirmed by TEM micrographs (Fig. 3 inset). We used the powerful AFM method (Figs. 4, 5, and 6) as well as CV (Fig. 7) and EIS (Fig. 8) analyses to study the surface architecture of the immunosensor.

It should be stated that MPA forms a covalently tight packed film on the gold electrode surface and effectively blocks the interfacial electron transfer between the redox couple in solution and the gold electrode surface, resulting in decreased redox current of the gold electrode modified with MPA as a self-assembly monolayer. Once the MPA modified gold electrode was functionalised with AuNPs@ SiO_2 , the electron

transfer rate improved efficiently in part due to the increased surface area of the modified electrode. We speculate that the greater size of AuNPs shown in AFM micrographs are due to possible aggregations of NPs with each other or the proximity of the functionalised spots on the surface in part due to the non-ordered primary silanisation (Fig. 4A, inset). CV results were confirmed by the EIS analyses, in which Nyquist plots displayed the same changes in the electron transfer process at the electrode-solution interface similar to that of the CV analyses. Based on the results obtained by EIS, the bare gold electrode exhibited a small semicircle in the Nyquist plot, which is a clear characteristic of the facile electron transfer of redox couple in the electrochemical process. Once MPA assembled on the gold electrode, it acted as an insulating layer that disturbed the interfacial electron transfer process between the electrode and the redox probe in the solution. The EIS data highlighted successful formation of MPA self-assembly on the electrode and also confirmed the results obtained by the CV analyses.

Next, the covalently attached amine-functionalised AuNPs@SiO₂ with carboxyl group of MPA through the formation of an amide bond was found to promote the electron transfer process.

Additional increase in current was observed upon conjugation of the MPA|AuNPs@SiO₂ modified gold electrode with CdSe QDs, which indicates formation of CdSe QDs-based conductive layer on the surface of the MPA|AuNPs@SiO₂/QD modified gold electrode. In fact, owing to great optical characteristics, QDs offer various applications for biosensing and bioimaging of various CMMs involved in different malignancies,⁴⁴ nonetheless they need to be properly functionalised and conjugated with appropriate targeting probes.⁴⁵

It should be expressed that the CdSe QDs (4 nm) were smaller than AuNPs@SiO₂ (20 nm). Hence, based upon interaction of CdSe QDs with AuNPs@SiO₂, it could be speculated that CdSe QDs randomly (with no pattern) settle on the AuNPs@SiO₂ modified gold electrode. Decoration of the MPA|AuNPs@SiO₂ modified gold electrode with CdSe QDs were found to increase the surface area and also act as a mediator because of their individual electronic characteristics, which in turn facilitates the electron charge transfer process by applying an effective potential at the surface of electrode (Fig. 8, curve d).

The R_{et} value was increased upon the conjugation of CA-125 mAb onto the electrode surface, perhaps due to the formation of an insulating protein layer on the surface of electrode. The immunosensor resulted in high specificity to CA-125 even in the presence of other competing proteins (Fig. 9). It also showed significant discrimination to various concentrations of CA-125, i.e., the higher the concentration of the CA-125, the larger the diameter of the semicircle of Nyquist plot (Fig. 10). The immunosensor displayed regeneration efficiency of 98.0% ± 1.2% (n=5) up to 22 cycles with an acceptable reproducibility and precision. Likewise, Fu *et al.* have used glycine-HCl (0.1 M, pH 2.0), acetonitrile (30 %), sodium hydroxide (50 mM) and sodium chloride (1.0 M) as regenerating reagents and showed that 0.1 M glycine-HCl (pH 2.0) could successfully regenerate CA-125 immunosensor up to 20 cycles with an acceptable reproducibility and precision.³³ Nano-architecture of the immunosensor constructed through the successive conjugation of AuNPs@SiO₂, CdSe QDs and anti CA-125 mAb onto the surface of the gold electrode enabled the sensitive detection of CA-125 with a LOD of 0.0016 U/mL and LDR of 0-0.1 U/mL as compared to some other CA-125 detecting biosensors (Table 2).

Table 2 Analytical characteristics of the immunosensor in comparison with different CA-125 detecting immunosensors

| Immunosensor materials | LOD (U/mL) | LDR (U/mL) | Method | Ref. |
|---|------------|----------------------|---------------------------|---------|
| AuNPs@SiO ₂ , CdSe QDs | 0.0016 | 0 - 0.1 | Impedimetric biosensor | Present |
| AuNPs Screen-printed electrode | 6.7 | 0 - 100 | Impedimetric immunosensor | 46 |
| Carbon paste interface; AuNPs; Thionine | 1.8 | 10 - 30 | Amperometric | 34 |
| Label-free immunosensor | 0.1 | 0.1- 40 | SPR | 32 |
| Molecular | 0.05 | 0.05- 40 | Capacitive | 47 |
| imprinted biosensor | 0.5 | 0.5-400 | DPV-EIS | 48 |
| Cellulose acetate; Colloidal AuNPs | 1.73 | 0 - 30 | DPV | 48 |
| Microfluidic origami device | 0.0074 | 0.01 - 100 | ECL | 49 |
| Screen-printed electrodes | | | | |
| Multiwall carbon nanotubes | 0.36 | 1.0 - 30 30 - 150 | CV | 50 |
| NafionTris(2,2'-bipyridyl)cobalt(III) | | | | |
| Carbon nanofiber | 1.8 | 2 - 75 | Amperometric | 51 |
| Prussian blue NPs, Colloidal AuNPs | 0.71 | 2.0 - 40 40 - 100 | DPV | 52 |

DPV: Differential pulse voltammetry; ECL: electrochemiluminescence; SPR: Surface plasmon resonance.

5. Conclusions

The early diagnosis of ovarian cancer is the cornerstone for the success of cancer treatment strategy.⁵³ To tackle this issue, several investigations have been accomplished to develop immunosensors for specific sensitive detection of CA-125,^{46, 48, 51, 54-56} which is an important CMM found in the serum of ovarian cancer patients.⁵⁷ Despite enormous efforts deployed to identify novel serum markers, no single marker has emerged as a serious competitor for the CA-125 as the most studied CMM expressed by 50-60 % of patients with early stage disease.⁵⁸ Although these studies resulted in promising diagnostic outcomes, most of them appeared to be sophisticated systems that often failed to provide a clear-cut detection of CA-125.⁴⁶ For example, Ravalli *et al.* reported a label free CA-125 detection based on gold nanostructured screen-printed method with LOD of 6.7 U/mL. In the current study, we have engineered a novel nanostructured immunosensor based on a simple cost-effective EIS method for the early detection of important oncomarker, CA-125. We have capitalised on a label and separation free EIS method to sense the faint electrochemical signals that were amplified through AuNPs@SiO₂ and CdSe QDs covalently conjugated onto the MPA-modified gold electrode. We found that the oncomarker CA-125 can specifically and sensitively be detected with LOD value of 0.0016 U/mL even in the presence of counterparts such as HSA, CEA and AFP. In comparison with other sensing methods (Table 2), the engineered immunosensor in our study resulted in very low LOD value with high reproducibility. As this immunosensor was decorated with AuNPs and CdSe QDs through covalent amide bond formation, we were able to detect faint signals of CA-125 complexation with the conjugated mAb. Based upon our findings, we envision the engineered

immunosensor as a potentially powerful diagnostic tool for the precise quantification of CA-125 in blood samples of ovarian cancer patients as well as any other malignancies that overexpress this oncomarker.

Acknowledgements

Authors are thankful to Ms Azami for the TEM technical support, Mr. Tabrizi for the human serum samples with patients' consents (approved by Tabriz University of Medical Sciences) from Nomooneh Lab. (Tabriz, Iran). Authors acknowledge the financial support by the Research Centre for Pharmaceutical Nanotechnology (RCPN) at Tabriz University of Medical Sciences. This study is part of a PhD thesis (ID: 9002) that was performed at RCPN, Faculty of Pharmacy, Tabriz University of Medical Science.

Notes and references

Electronic Supplementary Information (ESI) available: [Additional materials including Fig.s and discussion as described in the text are available for free at the website]. See DOI: 10.1039/b0000000x/

- J. Das and S. O. Kelley, *Anal Chem*, 2011, 83, 1167-1172.
- A. Ambrosi, M. T. Castañeda, A. J. Killard, M. R. Smyth, S. Alegret and A. Merkoçi, *Anal Chem*, 2007, 79, 5232-5240.
- X. Liu, Q. Dai, L. Austin, J. Coutts, G. Knowles, J. Zou, H. Chen and Q. Huo, *J Am Chem Soc*, 2008, 130, 2780-2782.
- G. Pampalakis and S. O. Kelley, *Analyst*, 2009, 134, 447-449.
- S. I. Stoeva, J.-S. Lee, J. E. Smith, S. T. Rosen and C. A. Mirkin, *J Am Chem Soc*, 2006, 128, 8378-8379.
- D. Tang and J. Ren, *Anal Chem*, 2008, 80, 8064-8070.
- E. Paleček and M. Fojta, *Talanta*, 2007, 74, 276-290.
- T. Sannomiya and J. Vörös, *Trends Biotechnol*, 2011, 29, 343-351.
- G. A. Rivas, M. D. Rubianes, M. C. Rodríguez, N. F. Ferreyra, G. L. Luque, M. L. Pedano, S. A. Miscoria and C. Parrado, *Talanta*, 2007, 74, 291-307.
- X. Cao, Y. Ye and S. Liu, *Anal Biochem*, 2011, 417, 1-16.
- K. Saha, S. S. Agasti, C. Kim, X. Li and V. M. Rotello, *Chem Rev*, 2012, 112, 2739-2779.
- N. Hildebrandt, *ACS Nano*, 2011, 5, 5286-5290.
- S. K. Arya and S. Bhansali, *Chem Rev*, 2011, 111, 6783-6809.
- B. V. Chikkaveeriah, A. A. Bhirde, N. Y. Morgan, H. S. Eden and X. Chen, *ACS Nano*, 2012, 6, 6546-6561.
- D. W. Kimmel, G. LeBlanc, M. E. Meschievitz and D. E. Cliffel, *Anal Chem*, 2011, 84, 685-707.
- M. I. Prodromidis, *Electrochimica Acta*, 2010, 55, 4227-4233.
- A. Vig, A. Radoi, X. Muñoz-Berbel, G. Gyemant and J.-L. Marty, *Sens Actuators B Chem*, 2009, 138, 214-220.
- A. Vig, X. Muñoz-Berbel, A. Radoi, M. Cortina-Puig and J.-L. Marty, *Talanta*, 2009, 80, 942-946.
- J. R. Siqueira Jr, L. Caseli, F. N. Crespilho, V. Zucolotto and O. N. Oliveira Jr, *Biosens Bioelectron*, 2010, 25, 1254-1263.
- B. Rezaei, T. Khayamian, N. Majidi and H. Rahmani, *Biosens Bioelectron*, 2009, 25, 395-399.
- R. Ghosh Chaudhuri and S. Paria, *Chem Rev*, 2011, 112, 2373-2433.
- S. Sarojini, A. Tamir, H. Lim, S. Li, S. Zhang, A. Goy, A. Pecora and K. S. Suh, *J Oncology*, 2012, 2012, 15.
- D. L. Meany, L. J. Sokoll and D. W. Chan, *Expert Opin Med Diagn*, 2009, 3, 597-605.
- R. C. Bast, *J Clin Oncol*, 2003, 21, 200-205.
- M. Ebrahimi, M. Johari-Ahar, H. Hamzeiy, J. Barar, O. Mashinchian and Y. Omid, *Bioimpacts*, 2012, 2, 91-95.
- H. Qiu, Y. Sun, X. Huang and Y. Qu, *Colloids Surf B Biointerfaces*, 2010, 79, 304-308.
- W. Haiss, N. T. Thanh, J. Aveyard and D. G. Fernig, *Anal Chem*, 2007, 79, 4215-4221.
- J.-F. Li, S.-B. Li, J. R. Anema, Z.-L. Yang, Y.-F. Huang, Y. Ding, Y.-F. Wu, X.-S. Zhou, D.-Y. Wu, B. Ren, Z.-L. Wang and Z.-Q. Tian, *Appl Spectrosc*, 2011, 65, 620-626.
- P. Liu, Q. Wang and X. Li, *J Phys Chem C*, 2009, 113, 7670-7676.
- W. W. Yu, L. Qu, W. Guo and X. Peng, *Chem Mater*, 2003, 15, 2854-2860.
- J. F. Li, S. B. Li, J. R. Anema, Z. L. Yang, Y. F. Huang, Y. Ding, Y. F. Wu, X. S. Zhou, D. Y. Wu, B. Ren, Z. L. Wang and Z. Q. Tian, *Appl Spectrosc*, 2011, 65, 620-626.
- S. Suwansa-ard, P. Kanatharana, P. Asawatreratanakul, B. Wongkittisuksa, C. Limsakul and P. Thavarungkul, *Biosens Bioelectron*, 2009, 24, 3436-3441.
- Z. Fu, H. Liu and H. Ju, *Anal Chem*, 2006, 78, 6999-7005.
- D. Tang, R. Yuan and Y. Chai, *Anal Chim Acta*, 2006, 564, 158-165.
- J. Yakovleva, R. Davidsson, A. Lobanova, M. Bengtsson, S. Eremin, T. Laurell and J. Emnéus, *Anal Chem*, 2002, 74, 2994-3004.
- J. N. Miller and J. C. Miller, *Statistics and Chemometrics for Analytical Chemistry*, Pearson/Prentice Hall, 2005.
- I. Taverniers, M. De Loose and E. Van Bockstaele, *Trends Analyt Chem*, 2004, 23, 535-552.
- C. Li, D. Sasaroli, X. Chen, J. Hu, R. Sandaltzopoulos, Y. Omid and G. Coukos, *Cancer biomarkers : section A of Disease markers*, 2010, 8, 253-271.
- J. Barar and Y. Omid, *Bioimpacts*, 2013, 3, 149-162.
- Y. Omid and J. Barar, *Bioimpacts*, 2014, 4, 55-67.
- Y. Park, J.-H. Lee, D. J. Hong, E. Y. Lee and H.-S. Kim, *Clin Biochem*, 2011, 44, 884-888.
- N. Scholler and N. Urban, *Biomarkers in medicine*, 2007, 1, 513-523.
- Y. Qi, M. Chen, S. Liang, J. Zhao and W. Yang, *Colloids Surf A Physicochem Eng Asp*, 2007, 302, 383-387.
- O. Mashinchian, M. Johari-Ahar, B. Ghaemi, M. Rashidi, J. Barar and Y. Omid, *Bioimpacts*, 2014, 4, 149-166.
- J. Barar and Y. Omid, *Bioimpacts*, 2014, 4, 3-14.
- A. Ravalli, G. P. dos Santos, M. Ferroni, G. Faglia, H. Yamanaka and G. Marrazza, *Sens Actuators B Chem*, 2013, 179, 194-200.
- S. Viswanathan, C. Rani, S. Ribeiro and C. Delerue-Matos, *Biosens Bioelectron*, 2012, 33, 179-183.
- L. Wu, J. Chen, D. Du and H. Ju, *Electrochim Acta*, 2006, 51, 1208-1214.
- S. Wang, L. Ge, M. Yan, J. Yu, X. Song, S. Ge and J. Huang, *Sens Actuators B Chem*, 2013, 176, 1-8.
- S. Chen, R. Yuan, Y. Chai, L. Min, W. Li and Y. Xu, *Electrochim Acta*, 2009, 54, 7242-7247.
- L. Wu, F. Yan and H. Ju, *J Immunol Methods*, 2007, 322, 12-19.
- S. Chen, R. Yuan, Y. Chai, Y. Xu, L. Min and N. Li, *Sens Actuators B Chem*, 2008, 135, 236-244.
- C. R. Morris, M. T. Sands and L. H. Smith, *Cancer Causes Control*, 2010, 21, 1203-1211.
- Z. Cui, D. Wu, Y. Zhang, H. Ma, H. Li, B. Du, Q. Wei and H. Ju, *Anal Chim Acta*, 2014, 807, 44-50.
- G. Wang, F. Jin, N. Dai, Z. Zhong, Y. Qing, M. Li, R. Yuan and D. Wang, *Anal Biochem*, 2012, 422, 7-13.
- W. Liu, Y. Zhang, S. Ge, X. Song, J. Huang, M. Yan and J. Yu, *Anal Chim Acta*, 2013, 770, 132-139.
- A. Gadducci, E. Sartori, P. Zola, F. Landoni, T. Maggino, N. Palai, A. Fanucchi and D. Katsaros, *Oncol Rep*, 1996, 3, 301-303.
- D. Sasaroli, G. Coukos and N. Scholler, *Biomark Med*, 2009, 3, 275-288.